Hindawi Publishing Corporation
International Journal of Rotating Machinery
Volume 2008, Article ID 147653, 9 pages
doi:10.1155/2008/147653

Research Article

Response of a Warped Flexible Rotor with a Fluid Bearing

Jim Meagher, Xi Wu, and Chris Lencioni

Department of Mechanical Engineering, California Polytechnic State University, San Luis Obispo, CA 93407, USA

Correspondence should be addressed to Jim Meagher, jmeagher@calpoly.edu

Received 21 June 2007; Revised 30 January 2008; Accepted 31 March 2008

Recommended by Agnes Muszynska

A two-complex-degrees-of-freedom model is developed and compared to experimental data for various amounts of rotor bow and its orientation to mass imbalance of the rotor. The equation of motion is developed by adding constant forces that rotate with the rotor to a Bently-Muszynska two-mode isotropic rotor model with a plane journal bearing. Diagnostic information discernable from probes at the bearing is explored and compared to midspan response, where previous research has concentrated. The model presented also extends earlier work by representing the effect of a nonrigid bearing. Good agreement between the analytical model and experiment demonstrates that the analysis presented can be useful to diagnose and balance residual shaft bow from probes located at the bearings, where vibration data are typically more available than midspan probes.

Copyright © 2008 Jim Meagher et al. This is an open access article distributed under the Creative Commons Attribution License, which permits unrestricted use, distribution, and reproduction in any medium, provided the original work is properly cited.

1. INTRODUCTION

Rotor bow can be a present in large horizontal rotors at rest for long periods, in misaligned rotors, or in rotors, where rub causes a thermal bow on the shaft. This can lead to instabilities, difficulty in balancing, and preload on bearings. Nicholas et al. [1] modeled shaft bow with a rotating force similar to imbalance and used a Jeffcott rotor model. Peak response and phase angle of bowed rotors were compared to straight shafts for various amounts of bow and bow orientation. The principal indicators of bow identified were phase angles other than 90 degrees at resonance and phase change variations during acceleration through resonance. Rao [2] used an equivalent analytical model and extensive simulations to develop a list of observations to help diagnose the presence of rotor bow. Both of these analytical studies used rigid bearings and the response at midspan, which is normally inaccessible. Flack and Rooke [3] used a transfer matrix method to study bowed rotor response for shafts with five different sets of fluid film bearings. The transfer matrix approach allowed multimass rotors to be analyzed. Direct comparisons to experimental data were also conducted for four different types of fluid bearings typically used in industrial turbo machines. Good agreement was reported between experiment and theory, but results were limited to midspan motion which is usually not available and only presented the case of imbalance and bow 180° apart. Model-based identification methods have increasingly been used to identify rotor bow [4], but they are necessarily more complicated, machine specific, and less general than the lumped parameter approach used herein. Numerical methods such as transfer matrices or finite elements allow individual machines to be modeled, but they do not easily provide parametric models or predicted responses that are transferable to other machines. The objective of this paper is two-fold: to provide a closed form solution for a bowed shaft response that includes a fluid bearing, and to compare midplane response to response at the bearing for the purpose of identifying shaft bow. Diagnostic information of machinery condition will thus be related to typical transducer measurement and location.

2. ANALYTICAL APPROACH

A Bently-Muszynska model [5] for a two mass system with a fluid bearing was modified to include rotor bow. The rotor model as depicted in Figure 1 has two lumped masses, a midspan disk and outboard journal, separated by a uniform flexible shaft. The rotor is supported by a stiff bearing inboard and a fluid bearing at the outboard end. The journal mass, M_2, operates in a fluid bearing characterized with lumped damping, D_B, and bearing stiffness, K_B. The average fluid circumferential velocity, λ, is the ratio of average fluid circumferential angular velocity over shaft angular velocity.

An imbalance is modeled at the midplane mass and is at an angle ao relative to the bow plane. The rotating forces fixed on the shaft that creates the bow effect, F_1 and F_2, are modeled using equilibrium corresponding to residual rotor deflection ro at midplane. These forces rotate synchronously and create the effect of a shaft bow amount of ro at the midspan disk, no deflection within the fluid bearing and no moment on the rigid bearing;

$$F_1 = (K_1 + K_2) r_0,$$
$$F_2 = \left(\frac{L_1}{L_1 + L_2}\right) F_1. \tag{1}$$

The corresponding equations of motion follow from the dynamic equilibrium depicted in Figures 1 and 2:

$$\begin{aligned} M_1 \ddot{\mathbf{r}}_1 + D_1 \dot{\mathbf{r}}_1 + (K_1 + K_2)\mathbf{r}_1 - K_2 \mathbf{r}_2 \\ = \mathrm{mr}_u \omega^2 e^{j(\omega t + \delta)} + F_1 e^{j(\omega t + \delta - a_0)}, \\ M_2 \ddot{\mathbf{r}}_2 + D_B \dot{\mathbf{r}}_2 + (K_2 + K_B - jD_B \lambda \omega)\mathbf{r}_2 - K_2 \mathbf{r}_1 \\ = F_2 e^{j(\omega t + \delta - a_0 + \pi)}. \end{aligned} \tag{2}$$

Assuming solutions of the form:

$$\mathbf{r}_1 = A_1 e^{j(\omega t + \alpha_1)},$$
$$\mathbf{r}_2 = A_2 e^{j(\omega t + \alpha_2)} \tag{3}$$

allows determination of the resulting motion at each mass:

$$\begin{aligned} A_1 e^{j\alpha_1} &= \frac{[K_2 + K_B - M_2\omega^2 + jD_B(1-\lambda)][\mathrm{mr}_u \omega^2 + F_1 e^{-ja_0}]e^{j\delta}}{Q} \\ &\quad + \frac{K_2 F_2 e^{j(\delta - a_0 + \pi)}}{Q}, \\ A_2 e^{j\alpha_2} &= \frac{K_2[\mathrm{mr}_u \omega^2 + F_1 e^{-ja_0}]e^{j\delta}}{Q} \\ &\quad + \frac{(K_1 + K_2 - M_1\omega^2 + j\omega D_1) F_2 e^{j(\delta - a_0 + \pi)}}{Q}, \end{aligned} \tag{4}$$

where Q denotes $[K_1 + K_2 - M_1\omega^2 + j\omega D_1][K_2 + K_B - M_2\omega^2 + jD_B\omega(1-\lambda)] - K_2{}^2$ and corresponding phase:

$$\alpha_i = \arctan\left[\frac{\mathrm{Im}(A_i e^{j\alpha_i})}{\mathrm{Re}(A_i e^{j\alpha_i})}\right], \quad i = 1, 2. \tag{5}$$

These equations were solved using Matlab for varying amount of bow and various orientations of the bow plane relative to mass unbalance. Single plane theoretical responses for a flexible rotor on stiff bearings are well known, [1, 2] but the cases presented here were tested experimentally and present results at the bearing, where vibration data are more readily available.

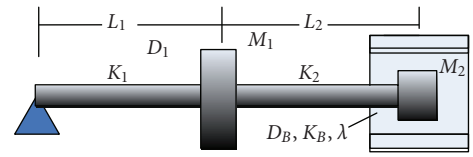

Figure 1: Two mass flexible rotor model.

Table 1: Simulation parameters.

parameters	values	units
M_1	1.802	Kg
M_2	0.291	Kg
L_1	0.225	m
L_2	0.183	m
D_1	20	N-s/m
D_b	2100	N-s/m
ε	2.3×10^{-4}	m
λ	0.48	
K_b	170000	N/m
δ	0	rad

3. SIMULATIONS

The equations above were solved using the parameters listed in Table 1. The values of these parameters were determined experimentally as discussed in the following section. Numerical comparison of the vibration amplitude at the midplane to the response at the bearing is shown in Figure 3. At midspan the effect of self-balancing is evident. Depending upon the ratio of bow to eccentricity, when bow and imbalance are 180° apart, there will be a speed at which these effects cancel. For a Jeffcott rotor model the self-balancing speed occurs at $\omega^2 = R_{0*}\omega_n{}^2$ for ao = 180°. This occurs at approximately the same speed, when a fluid bearing is present. This indicator of bow however is not apparent at the fluid bearing. Response at the bearing appears to be solely from eccentricity.

A three-dimensional map of this effect is shown in Figure 4. The effect of imbalance alone is represented by curves along Ro = 0. As bow is increased a self-balancing speed appears at the midplane. This speed increases with bow and has a minimum overall response when Ro = 1, which is the case where the eccentricity and bow are equal. The response at the fluid bearing also has a minimum response for Ro = 1 but not self-balancing. The associated phases for the responses in Figure 4 are shown in Figure 5. The phase of a bowed shaft is quite different than that of a straight shaft with imbalance. The most notable feature is the 180° phase jump that occurs when the response shifts from a low speed response to bow to that dominated by imbalance. At the balance speed the effects is cancelled. Below and above this speed the phase is toward either the bow or imbalance which is 180° apart for this case.

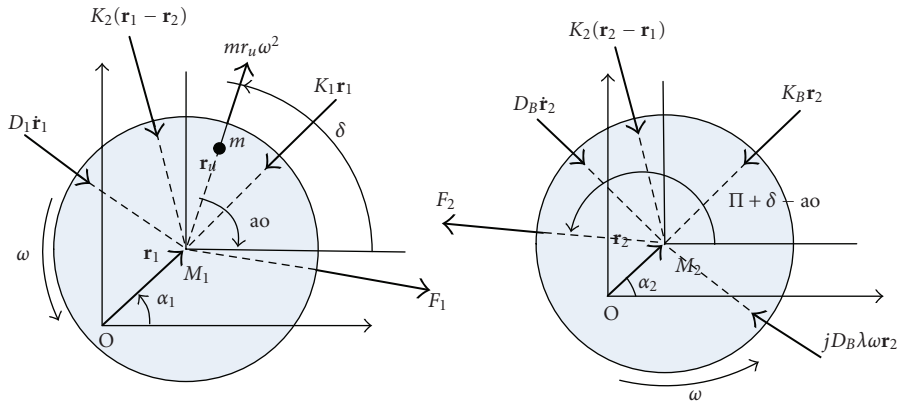

FIGURE 2: Lumped parameter modeling of forces in each plane.

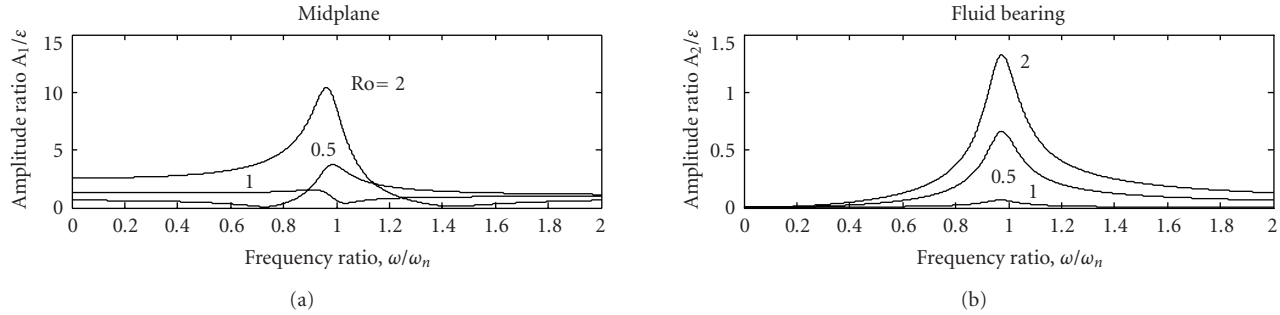

FIGURE 3: Response curves with bow opposite imbalance for various amounts of bow, Ro.

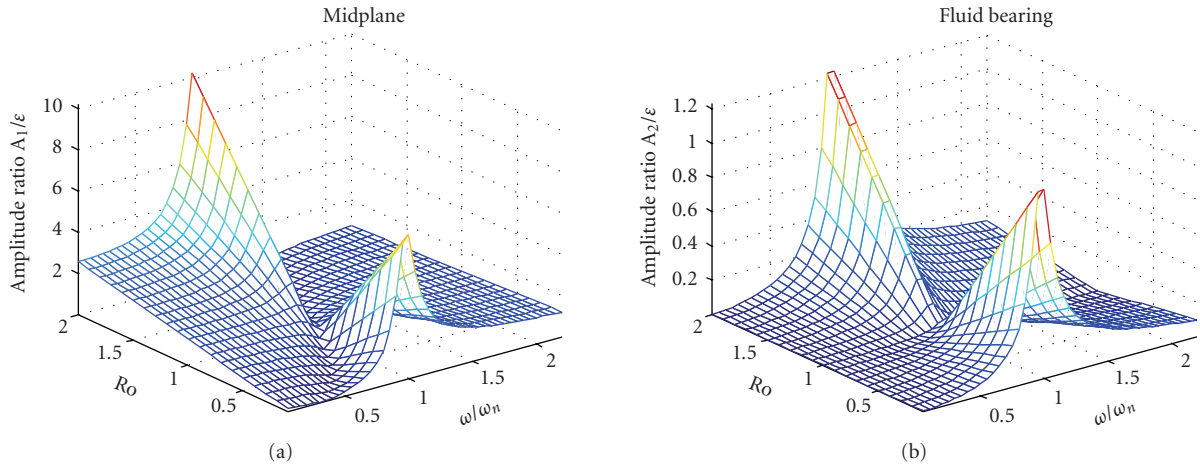

FIGURE 4: Response amplitudes at midspan (a) and at the fluid bearing (b) for an imbalanced rotor with varying amount of bow.

Figure 6 illustrates how the position of the central disk along the shaft does not affect the self-balancing speed. For this model the effective shaft stiffness remains the same. The peak response however gets smaller as the disk gets closer to the fluid bearing. The response amplitude at the fluid bearing does not monotonically decrease in the same way nor does the amplitude vary as much. Increased damping is evidenced in both planes by the broadening of the response curve. Since an isotropic shaft was assumed variation in the parameter L_1/L is equivalent to changing the shaft segment stiffness on either side of the central disk. Figure 7 shows a fuller description of the response

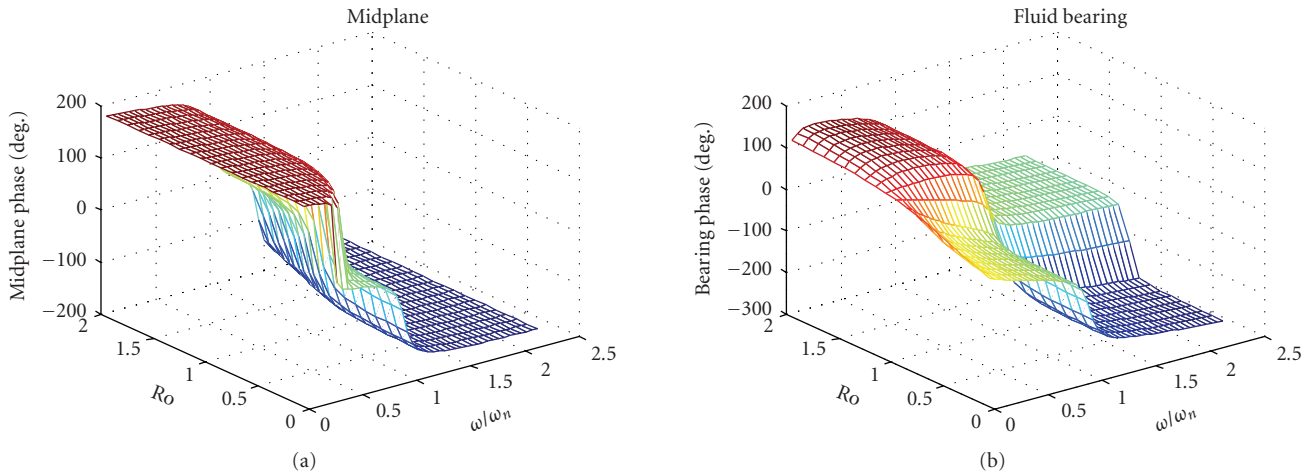

FIGURE 5: Phase at midspan (a) and at the fluid bearing (b) for an imbalanced rotor with varying amount of bow. The bow plane is opposite the imbalance.

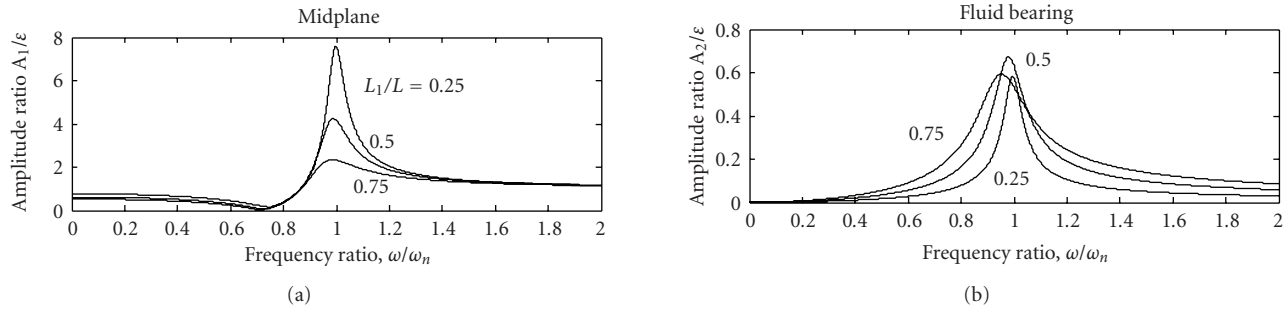

FIGURE 6: Response curves for various locations of disk. Ro = 0.5, ao= 180°.

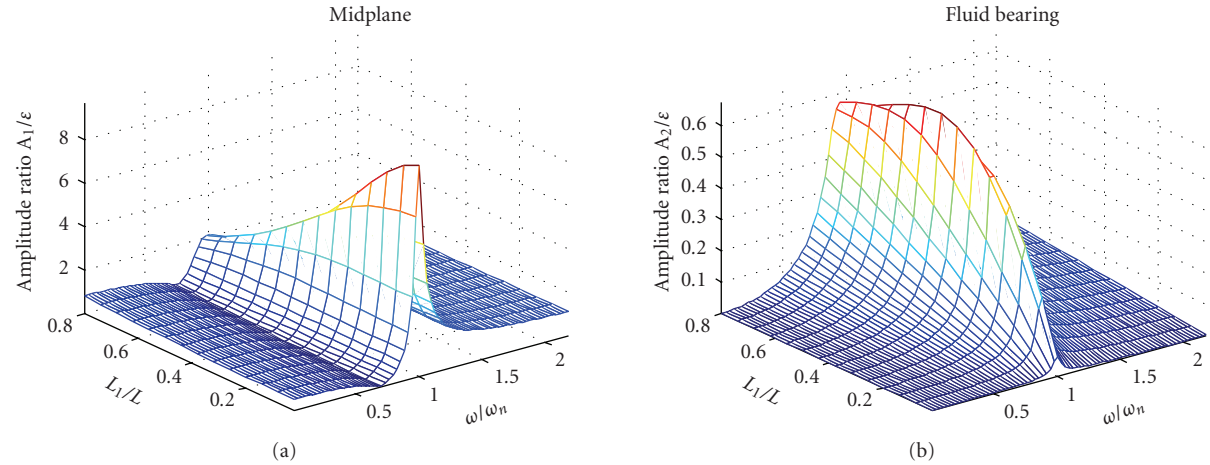

FIGURE 7: Response amplitudes at midspan (a) and at the fluid bearing (b) for an imbalanced rotor with Ro = 0.5 for various locations of the midspan disk.

amplitude variations with the associated phase changes shown in Figure 8. The peak midplane response occurs when the central disk is near the rigid bearing. The effective damping is reduced and the amplitude ratio is four times that compared to the disk near the fluid bearing. The phase jump at the self-balancing speed is apparent for all length ratios. The response at the fluid bearing has a maximum for the central disk to be at the center of the shaft. The phase changes seen at the fluid bearing are more gradual.

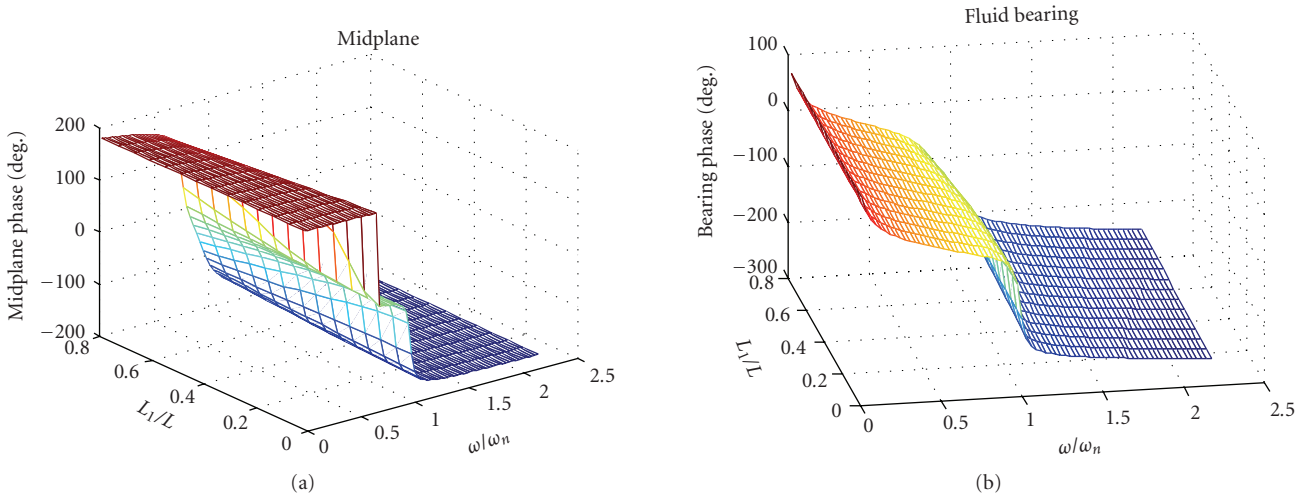

FIGURE 8: Phase at midspan (a) and at the fluid bearing (b) corresponding to the frequency response plots shown in Figure 7.

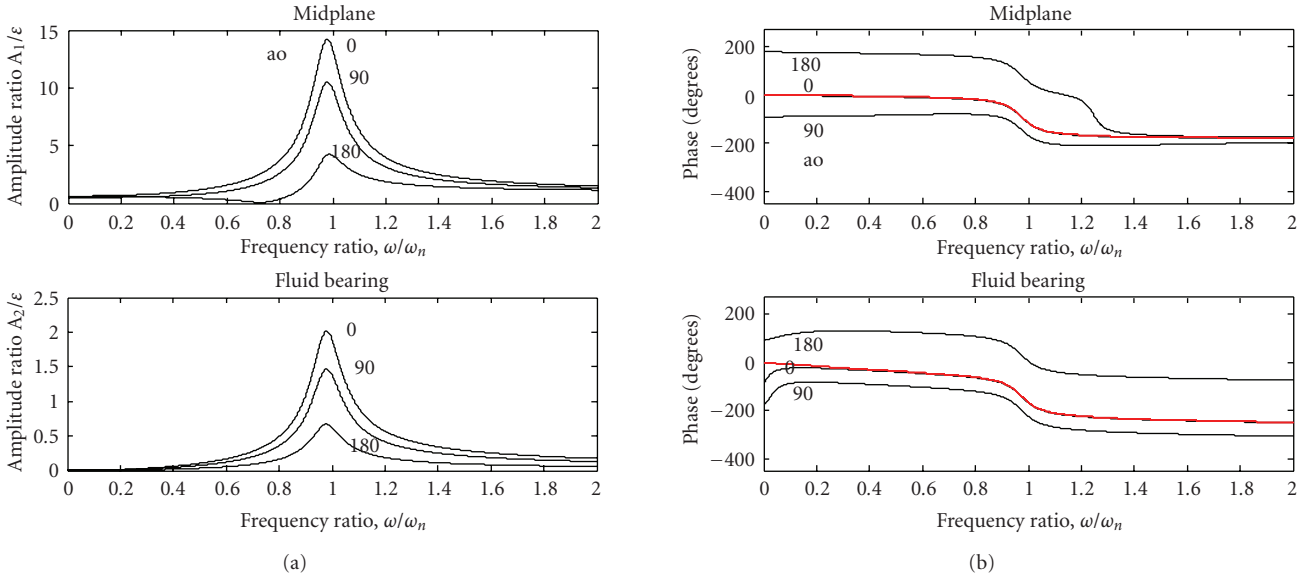

FIGURE 9: Amplitude (a) and phase response (b) for various bow orientations relative to the imbalance plane. Ro = 0.5. The curve in red is for a rotor with imbalance but no bow.

Figure 9 depicts the effect of the relative orientation between the bow plane and the imbalance plane. The midplane response amplitude plot, Figure 9(a), has zero amplitude at a speed ratio of 0.7 for ao = 180°. This self balancing does not occur at the outboard bearing for any relative orientation and only occurs at 180° at the midplane. At 0° difference, the bow and imbalance act in phase to have the largest response. The low-speed phase measured at midplane, Figure 9(b), is a good diagnostic for bow location. At low speed the response phase is equal to bow orientation. Unfortunately, the low amplitude of vibration makes the accurate measurement of phase difficult as shown later in Figure 15. The phase jump evident in Figure 9(a) for the midplane, with ao = 180°, is another indicator of self-balancing. At low speed the phase at the fluid bearing lags the bow plane by 90° but as the shaft speed increases the phase changes due to the fluid tangential force, $jD_B\lambda\omega\mathbf{r}_2$. The lines in red of Figure 9 are for imbalance without any bow. This shows the agreement of low-speed phase at midspan and a 90° phase shift at the fluid bearing.

Figures 10 and 11 depict a more complete description of the parameter variation effects shown in Figure 9. The response amplitudes decrease monotonically at midplane and at the bearing as the bow to imbalance orientation increases from aligned to 180° apart. Self-balancing occurs for a very particular case and is visible only at midplane.

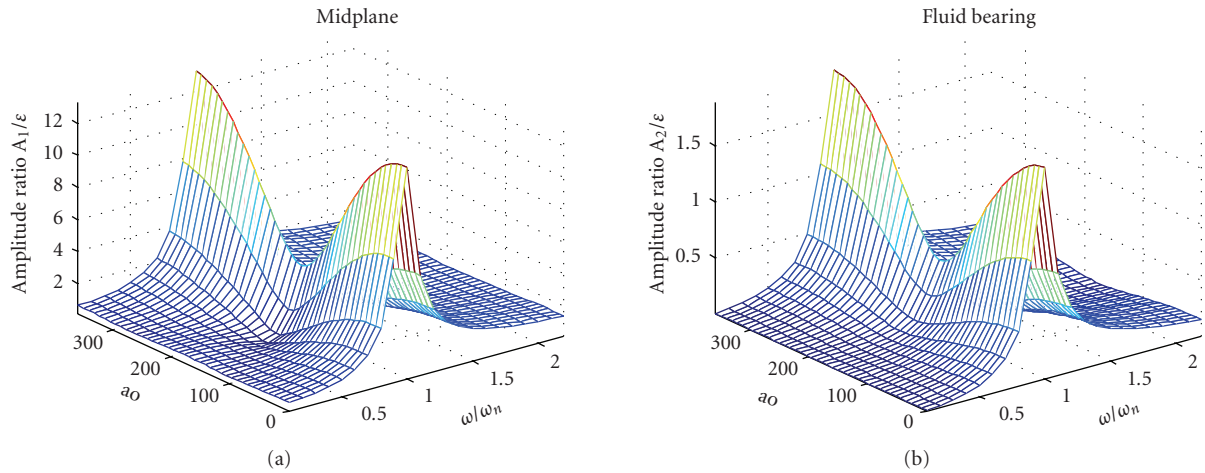

Figure 10: Response amplitude at midspan (a) and at the fluid bearing (b) for various orientations of bow with repect to imbalance. Ro = 0.5.

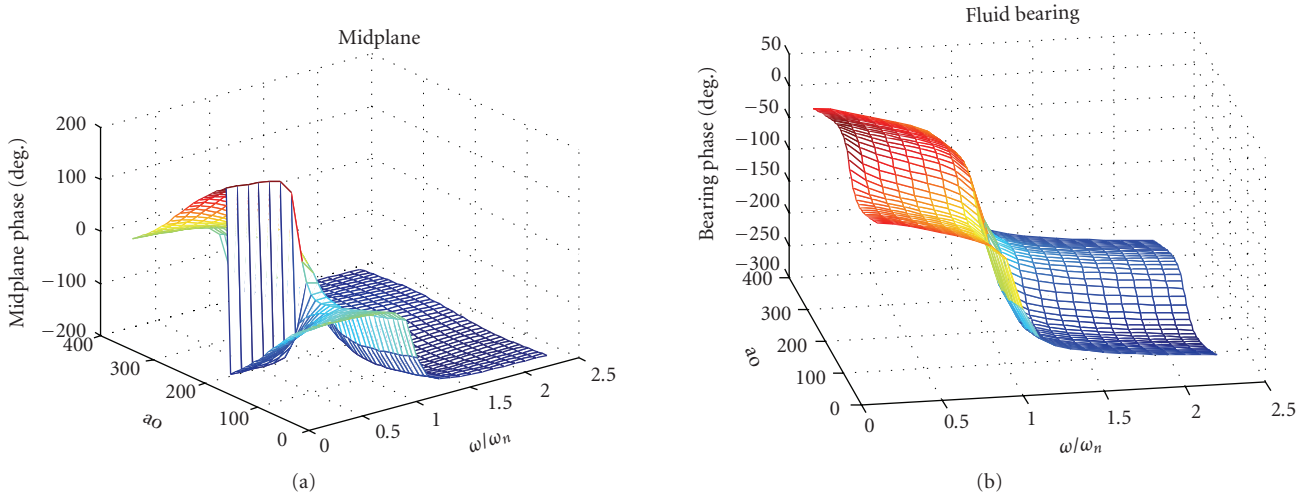

Figure 11: Phase at midspan (a) and at the fluid bearing (b) for various orientations of bow with respect to imbalance. Ro = 0.5.

Phase jump at midplane is also shown to be an isolated occurrence at midplance from Figure 11.

4. EXPERIMENTAL RESULTS

An RK4 Bently Nevada Rotor kit shown in Figure 12 was used for experimental measurements. The rotor is driven through a flexible coupling by an electric motor with a speed controller. The speed range of testing was from a slow roll of 250 rpm up to approximately 3500 rpm, where whirl instability was observed. Shaft lateral vibrations were measured with two sets of proximity probes in horizontal and vertical orientations at the midspan disk and at the fluid journal bearing, Figure 12(b). The fluid bearing used was the standard pressurized fluid bearing that comes with the Bently Nevada RK4 rotor kit. It has a 1 inch diameter lucite journal and 15-mil diametral clearance. The bearing has four oil injection ports spaced evenly around the bearing. The pump pressure was set to 10 psi.

Before testing, a 10 mm rotor was permanently bowed in a hydraulic test machine. The rotor was then carefully balanced in order for the high speed imbalance response to equal the low speed bow response with self-balancing at the critical speed. Theoretically for a Jeffcott rotor model this occurs, when the bow plane and imbalance are 180° apart with $R_0 = 1$. As shown in Figure 13, this response is accurately modeled by the proposed lumped parameter model except Ro was set to 0.87 due to differences in predicted response with the current model. This case is used as a baseline for parameter identification and is critical in establishing orientation of the imbalance plane relative to the bow plane as well as for determining the amount of residual imbalance.

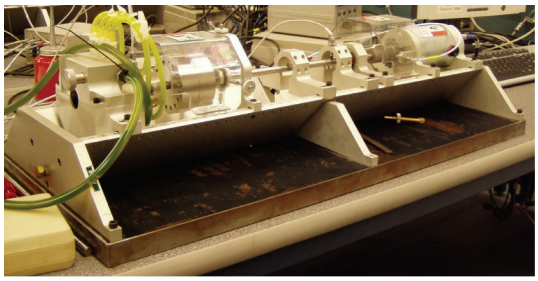

(a)

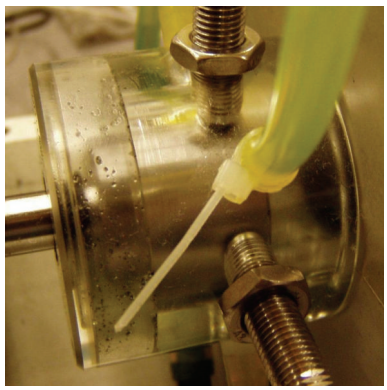

(b)

Figure 12: Experimental setup (a) with fluid bearing on the left and variable speed motor on the right, (b) close-up of fluid bearing showing supply lines and proximity probes.

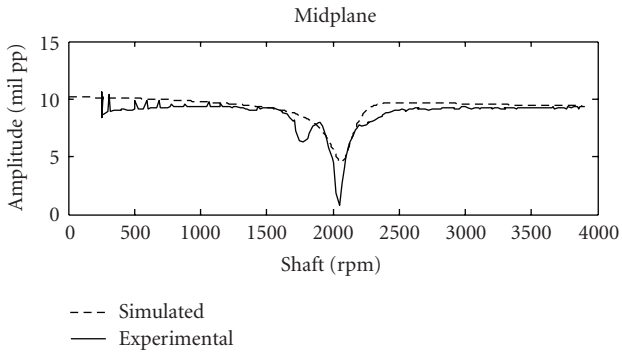

Figure 13: Bowed rotor experimental (exp.) and simulated (sim.) response.

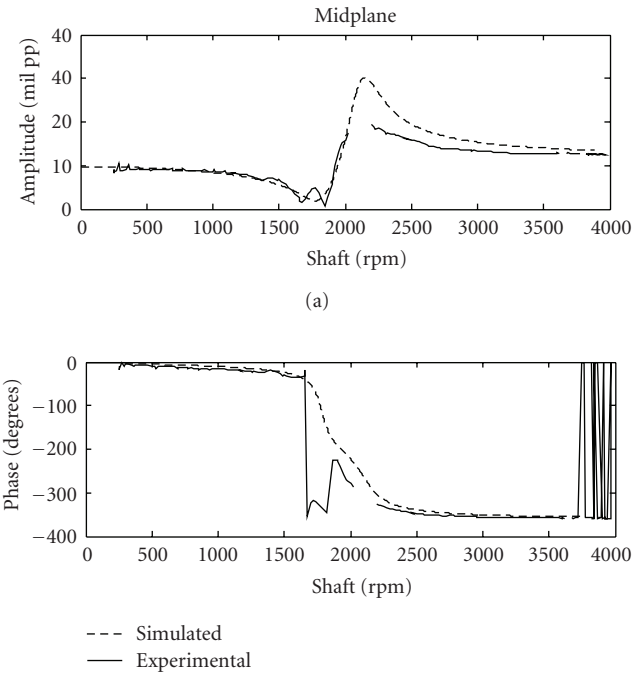

(a)

(b)

Figure 14: Synchronous response of a bowed rotor at midplane disk. Ro = .64, ao = 180°. Drop out of data near 2000 rpm is due to displacement exceeding transducer range. Phase wrap evident in the experimental plot around 1700 rpm and above 3500 rpm is due to software that adds 360° for phase ranges beyond 360°.

Subsequent simulations for different bow factor and bow orientation use the same parameters as listed in Table 1 except for imbalance orientation and eccentricity which were experimentally modified using additional imbalance masses added to the rotor disk.

By identifying this as a reference configuration, the imbalance plane orientation can be changed with the addition of imbalance masses. The stiffness, mass, and damping factor used in simulations are based on values obtained from nonsynchronous perturbation testing [6]. Using this method requires a known radial perturbation force. This was supplied by a free spinning perturbator located adjacent to the rotor mass. The speed of the perturbation force is controlled independently of the rotor speed using a separate motor speed controller to control the speed of a freely spinning imbalanced disk mounted on the rotor. A plot of direct dynamic stiffness and quadrature stiffness allows the determination of modal mass, damping, and stiffness [6]. After some modification to match the reference experimental data shown in Figure 13 these parameters were held constant. This is justified from the experimental frequency responses shown in Figures 14–17 which reveal a single mode of response in the speed range tested.

The case of self-balancing prior to the critical speed is shown in Figures 14 and 15. Additional imbalance mass was added opposite the bow plane to increase the eccentricity. This decreased the bow factor while maintaining the 180° separation between the bow plane and the imbalance plane. At low speeds the bow response is dominant and is characterized by high whirl amplitude. The amplitude reaches a minimum when the bow response and imbalance cancel. After resonance, the response is dominated by the imbalance response and asymptotically approaches the eccentricity. This is as predicted by earlier models [1, 2]. The limitation of earlier models is shown in Figure 15, where the response at the bearing is depicted. The self-balancing speed is no longer evident and the response is not easily identified as a bowed

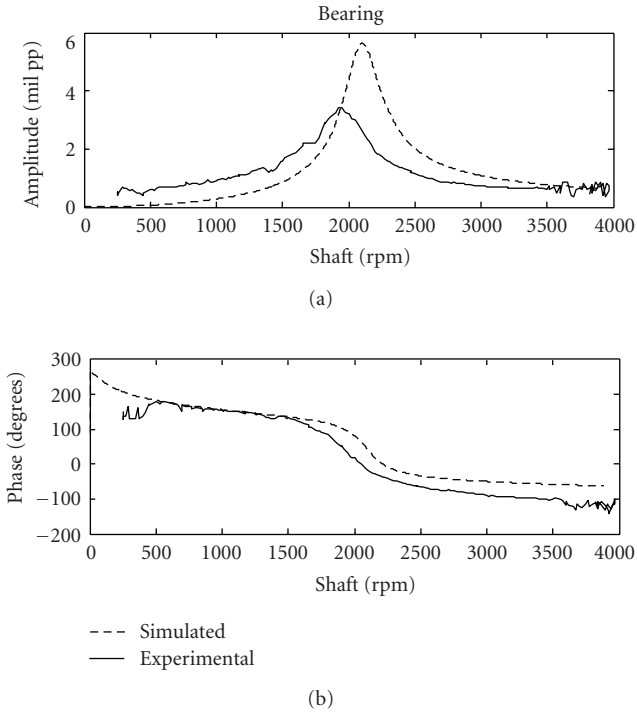

Figure 15: Synchronous response of a bowed rotor at outboard bearing. Ro = .64, ao = 180°.

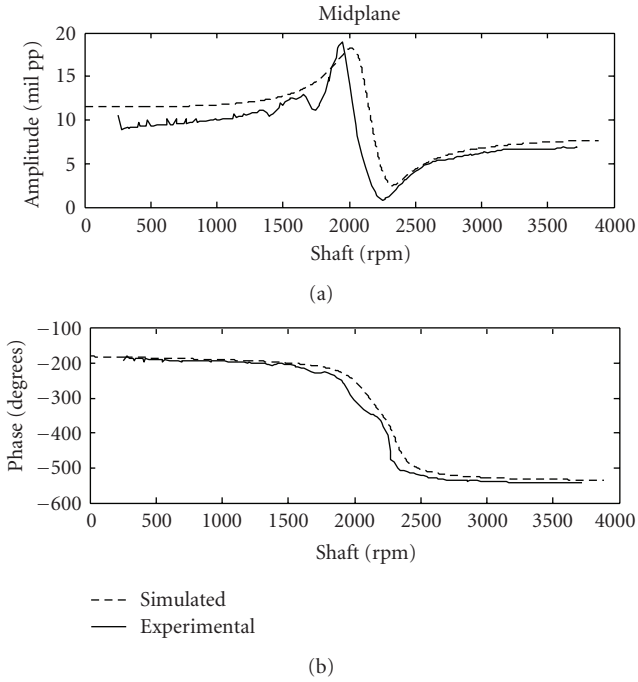

Figure 16: Synchronous response of a bowed rotor at midplane disk. Ro = 1.09, ao = 180°.

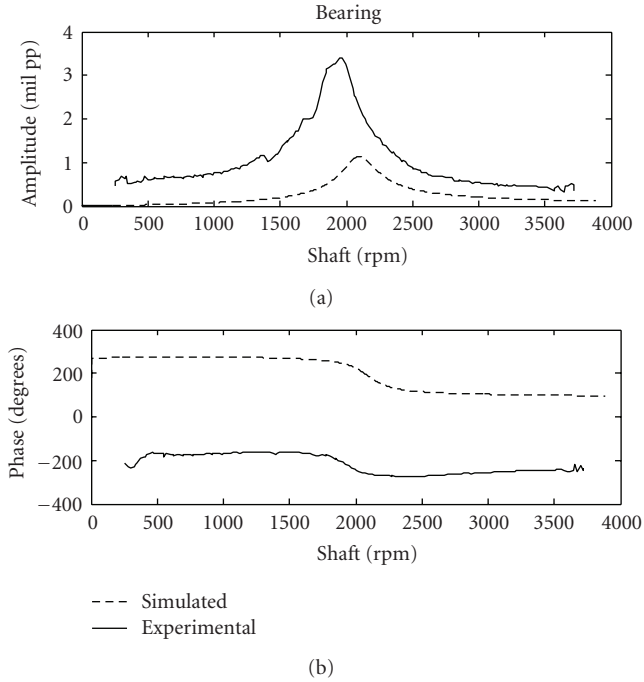

Figure 17: Synchronous response of a bowed rotor at outboard bearing. Ro = 1.09, ao = 180 degrees.

rotor. The low-speed response asymptote does not as clearly indicate bow as does the midplane response.

Similar differences between midplane and outboard measurements occur when masses opposite the bow plane are removed. This increases the bow factor and moves the self-balancing speed above the critical speed as shown in Figure 16. Removing imbalance masses increases the bow factor by decreasing the eccentricity. Once again the simulation and experimental response are well matched in both planes, but single plane models would not predict the presence of bow from the bearing data, which illustrates the difficulty of diagnosing a bowed rotor from the bearing response.

5. SUMMARY

A closed-form parametric model of a flexible bowed shaft with imbalance is presented. The mathematical model agrees with experimental measurements and extends earlier models by including an outboard fluid bearing with response predicted at the bearing, where response data is more typically available. Self-balancing, as predicted by Jeffcott rotor models, occurs as well as for a rotor with a fluid bearing, but is not apparent using probes at the fluid bearing. Diagnostic indicators for bow such as self-balancing or phase jump which can be seen at midspan are not apparent at the bearing. However, low-speed runout at the fluid bearing can be used to indicate residual rotor bow, but it is not as obvious as measurements made from midspan probes. The low-speed phase at either the fluid bearing or midspan indicates the bow angle with respect to the imbalance. Good agreement between the analytical model and experiment demonstrates that the analysis presented can be useful to diagnose and balance residual shaft bow from probes located at the bearings, where vibration data are typically more available than midspan probes.

NOMENCLATURES

A_1, A_2: Synchronous response amplitude in planes 1 and 2 (m).
D_1, D_B: Damping at inboard disk and outboard journal bearing (N-s/m).
F_1, F_2: Forces that bow the shaft (N).
K_1, K_2, K_B: Stiffness of shaft segments and journal bearing (N/m).
L_1, L_2: Length of shaft segments on either side of disk (m).
L: Total length of shaft (m).
M_1, M_2: Mass of midplane disk and journal mass (kg).
ao: Angular location of bow with respect to imbalance (rad).
ε: Eccentricity of M_1 (m).
mr_u: Imbalance, equivalent to $M_1\varepsilon$ (N-m).
Ro: Bow factor, ratio of bow to eccentricity ro/ε.
ro: Bow (m).
$\mathbf{r}_1$, $\mathbf{r}_2$: Complex displacements in plane 1 and 2.
t: Time (s).
α_1, α_2: Phase (rad).
δ: Angular location of mass imbalance at $t = 0$.
λ: Fluid circumferential average velocity ratio.
ω: Angular velocity of rotor (rad/s).
ω_n: $\sqrt{(K_1 + K_2)/M_1}$ (rad/s).
j: $\sqrt{-1}$.

ACKNOWLEDGMENT

The authors wish to acknowledge the Donald E. Bently Center for Engineering Innovation at California Polytechnic State University San Luis Obispo for supporting this work.

REFERENCES

[1] J. C. Nicholas, E. J. Gunter, and P. E. Allaire, "Effect of residual shaft bow on unbalance response and balancing of a single mass flexible rotor: part I—unbalancing response: part II—balancing," *Journal of Engineering for Power*, vol. 98, no. 2, pp. 171–181, 1976.

[2] J. S. Rao, "A note on Jeffcott warped rotor," *Mechanism and Machine Theory*, vol. 36, no. 5, pp. 563–575, 2001.

[3] R. D. Flack and J. H. Rooke, "A theoretical-experimental comparison of the synchronous response of a bowed rotor in five different sets of fluid film bearings," *Journal of Sound and Vibration*, vol. 73, no. 4, pp. 505–517, 1980.

[4] N. Bachschmid, P. Pennacchi, and A. Vania, "Identification of multiple faults in rotor systems," *Journal of Sound and Vibration*, vol. 254, no. 2, pp. 327–366, 2003.

[5] D. E. Bently and C. T. Hatch, *Fundamentals of Rotating Machinery Diagnostics*, Bently Pressurized Bearing Press, Minden, Nev, USA, 2002.

[6] D. E. Bently, D. W. Mathis, G. R. Thomas, and G. G. Nichols, "Experimental determination of rotor bearing parameters and fluid inertia effect using nonsynchronous perturbation testing," in *Proceedings of the 2nd International Symposium on Stability Control of Rotating Machinery (ISCORMA-2)*, Gdansk, Poland, August 2003.